

A Detailed Analysis of the Nonlinear Dynamics of the Electric Step Motor

J. Reiss, F. Alin*, M. Sandler and B. Robert*

Dept. of Electronic Engineering, Queen Mary, University of London
 Mile End Road, London E14NS United Kingdom
 Phone: +44 (0)207-882-5528, +44 (0) 207-882-7680 Fax: +44 (0)207-882-7997
 Email: josh.reiss,mark.sandler@elec.qmul.ac.uk

*Laboratoire d'Automatique et de Microélectronique, UFR Sciences Exactes et Naturelles
 Moulin de la Housse BP 1039, 51687 Reims Cedex 2, France
 Phone: +33 (0) 3 26 91 32 48, +33 (0) 3 26 91 84 23 Fax: +33 (0) 3 26 91 31 06
 E-mail : francois.alin,bruno.robert@univ-reims.fr

Abstract

The electric step motor is an electromechanical device which converts electrical pulses into discrete mechanical movements. The shaft of the motor rotates in discrete increments when command pulses are applied in the proper sequence. The dynamic behavior of this motor is of great importance, since instabilities lead to velocity fluctuations that are unacceptable in many applications. It is a major limitation to the development of high performance open-loop step motor system. The dynamics of a hybrid step motor is studied by using the tools of chaos theory and time series analysis. Lyapunov exponents, fractal dimension and other empirical quantities are determined from experimental data. Particular attention is paid to issues of stationarity in the system. We show that the electric step motor may function as a low-dimensional chaotic system. As such, chaotic control techniques may be applied that allow this motor to operate effectively within the chaotic regime.

Keywords: Stepper motor, electric step motor systems, chaos, nonlinear dynamics, time series analysis

1. Introduction

The electric step motor is a type of motor that provides incremental motion, or steps, in response to pulses of current that alternately change the polarity of the stator poles. The main advantage of an electric step motor is its open-loop operation. That is the position control can be achieved without shaft position feedback. The shaft can be stopped in any position with a high degree of accuracy, thus producing incremental displacements. It is used in numerous applications such as printers, hard disks, toys and robots.

As depicted in Figure 1, the stator has windings, 1 and 3 in series fed by the voltage U_a , and 2 and 4 in series fed by the voltage U_b . I_a is the current in the windings 1 and 3 and I_b is the current in the windings 2 and 4. The rotor has permanent magnets. Torque is developed by the tendency of the rotor and stator magnetic fields to pull into alignment according to the sequential feeding of the phases. If phase **a** (windings 1-3) is fed, stator induction is horizontal and the rotor is also horizontal (Figure 1, part a). If phase **b** (windings 2-4) is fed, stator induction is vertical and the rotor turns one step (Figure 1, part b). If the two phases are fed simultaneously, induction produced by the stator has an intermediate position, the rotor turns a half step. Phases are switched alternately. Consider the following cycle:

- 1 ($I_a = I_n, I_b = -I_n$), 2 ($I_a = I_n, I_b = I_n$),
- 3 ($I_a = -I_n, I_b = I_n$), 4 ($I_a = -I_n, I_b = -I_n$)

The rotor has four stable positions during the switch cycle, which are $-p/4$, $p/4$, $3p/4$, and $5p/4$. This is the supply mode that is most frequently used and is called mode 2.

The torque has two origins. First, teeth on the stator and on the rotor create a variable resistance. Second, the magnetization of the rotor creates an interaction between the rotor magnets and the stator currents. According to the physical phenomenon responsible for the torque, motors can be classified as variable reluctance motors, permanent magnet motors, or hybrid motors. Variable reluctance motors have teeth on the stator and on the rotor, but no permanent magnet on the rotor. In this case, the torque is due to the variable resistance. Permanent magnet motors have rotors radially magnetized as described in Figure 1.

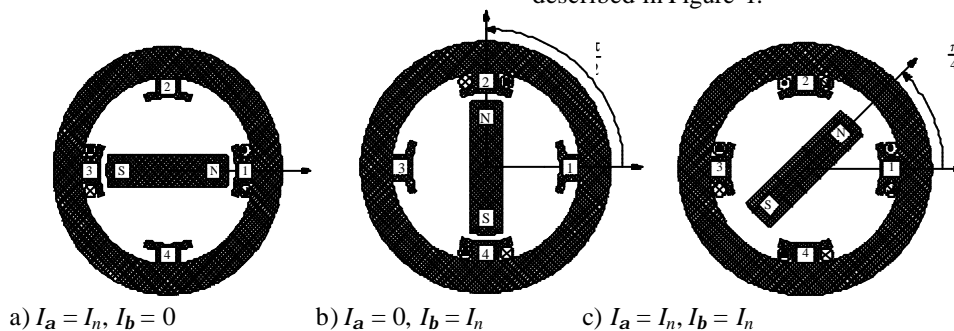


Figure 1. Principle of the step motor

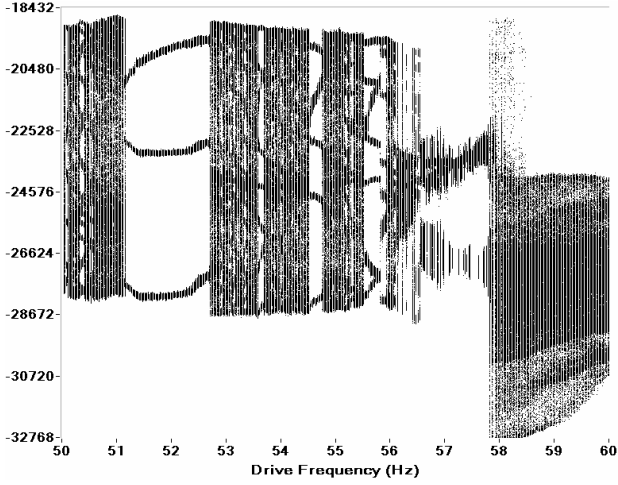


Figure 2. Bifurcation diagram. 1000 consecutive points are plotted vertically for data gathered at 20mHz intervals from 50 to 60Hz.

The motor that we consider is a commercial motor, the Crouzet 82940 002. It belongs to the third type of stepper motor, the hybrid motors. The hybrid motors are the most common type. The stator has salient poles, with two phases. The rotor includes a cylindrical axial permanent magnet, mounted on the shaft and placed between two iron disks with teeth. Due to the axial magnet, Z_r teeth of the same disk have identical polarity, that is, one disk bears Z_r south poles and the other bears Z_r north poles. Teeth of the disks are shifted an electric angle \mathbf{p} , so a stator tooth faces alternately north and south poles.

The studied motor has $Z_r=12$ teeth on each rotor disk, so the rotor has 24 poles. It is fed in mode 2. That is, U_a and U_b are square voltages with a phase shift of $\pi/2$. Hence the motor has 48 stable positions. It is a 48 steps per tour motor, with a stepping angle of $360/48=7.5^\circ$.

The motor is supposed to operate at synchronous speed. The rotation speed is usually proportional to the supply frequency. But when the frequency increases, erratic behavior occurs, leading to a loss of synchronism. Usual studies tend toward elaborate motor control that avoids this problem. It is hoped that a nonlinear dynamics approach will yield a better understanding and better controls.

We study a hybrid step motor, two-phased, 48 steps/tr. The motor is unloaded. The two phases, respectively noted \mathbf{a} and \mathbf{b} , are supplied by U_a and U_b in mode 2, i.e. two square voltages shifted of $\mathbf{p}/2$. The motor is modeled as follows

$$L\dot{I}_a = U_a(t) - RI_a + K_e\Omega_m \sin(Z_r\mathbf{q}_m) \quad (1)$$

$$L\dot{I}_b = U_b(t) - RI_b - K_e\Omega_m \cos(Z_r\mathbf{q}_m) \quad (2)$$

$$\dot{\mathbf{q}}_m = \Omega_m \quad (3)$$

$$J\dot{\Omega}_m = K_h I_b \cos(Z_r\mathbf{q}_m) - K_h I_a \sin(Z_r\mathbf{q}_m) - K_d \sin(4Z_r\mathbf{q}_m) - F\Omega_m - \Gamma_c \quad (4)$$

I_a and I_b : currents in phases \mathbf{a} and \mathbf{b} , \mathbf{q}_m : angular position, Ω_m : rotation speed, $R=45\Omega$ (phase resistance), $L=275\text{mH}$ (phase inductance), $Z_r=12$ (teeth number), $J=$

18.10^{-6} kgm^2 (inertia), $K_h=K_e=0,463 \text{ Nm/A}$ (emf constant and torque constant), $K_d=16 \text{ mNm}$ (detent torque), $F=10^{-4} \text{ Nms/rd}$ (friction coefficient), $\Gamma_c=0$ (load torque).

In previous work it has been shown that this motor might exhibit chaotic behavior.[1, 2] We will analyze time series from both the model and the experiment. We will use a variety of techniques from chaotic time series analysis to show that the system is indeed chaotic and that there is considerable agreement between the model and the experiment.

The analysis that follows concentrates on the simulation, two 100,000 point experimental flow data sets with drive frequencies 50.75 Hz and 59.75Hz, and a series of 20,000 point Poincare sectioned data sets. Results from this data will be analyzed and compared to show the dynamics of the experiment and how these differ from the dynamics of the model. Estimates of current were gathered through a Hall-effect probe connected to a digital oscilloscope. In the results that follow, units are not given on the current measurements since they have been scaled and transformed by the data acquisition system.

The experimental data sets consist of two columns of data, each column corresponding to the current in one phase of the motor. The sectioned data consists of 500 individual data sets ranging from a drive frequency of 50Hz to 60 Hz, incremented by 20mHz. Figure 2 depicts a bifurcation diagram derived from the sectioned data. It exhibits band structures and periodic regimes interspersed with complex dynamics. Such a bifurcation diagram is typical of many chaotic systems.

2. Nonstationarity and Long-term dynamics

A few simple tests were performed that would identify strong drifts in the data. Sliding windows of varying length were applied to the sectioned data sets. The mean of each window was measured and plotted as a function of the window's position. Results of the drift in the mean are depicted in Figure 3.

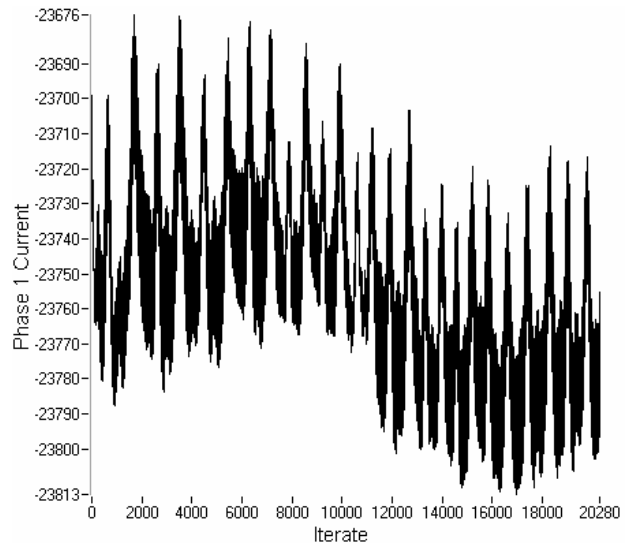


Figure 3. Nonstationary behavior of the data mean. Plotted are estimates of the mean for overlapping windows of length 200 from the 50.04Hz Sectioned data.

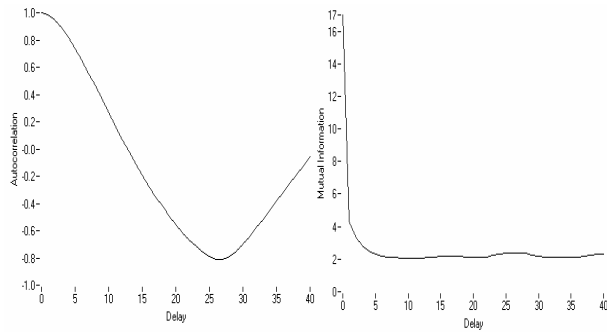


Figure 4. Two techniques for estimating an embedding delay from the 50.75Hz flow data. The first method is to choose the first minimum of the mutual information function. The second uses the first zero crossing of the autocorrelation function. Both methods suggest a delay of approximately 13.

It can be clearly seen that there is long-term cyclic behavior in this data. The mean value undergoes a fluctuating trend that does not appear to be random. This fluctuation is quite small in relation to the full extent of the data ($\sim 1\%$) but it may affect the results of chaotic time series analysis methods. It is doubtful that this is caused by parameter drift since that does not account for the cyclical nature. More likely, it is inherent to the system and is the result of long-term dynamics that must be taken into account. Similar plots at other frequencies also often indicated the presence of long-term dynamics and possibly parameter drift. This was also confirmed by the measurement of other statistical quantities such as standard deviation for windowed data.

3. Embedding Parameters

A reasonable value for the delay may be suggested either by the first zero crossing of the autocorrelation function or by the first minimum of the mutual information function[3, 4], as either value is plotted as a function of delay. The mutual information often gives a better value because it takes nonlinear correlations into account. Mutual information was calculated efficiently using a method described in Reiss, et al.[5] However, for the step motor data, the mutual information function and the autocorrelation function were in perfect agreement. As shown in Figure 4 both values suggested a delay of approximately 13. Other estimates of the appropriate delay from any of the flow data sets gave values between the range of 9 to 16. This was in agreement with visual inspection since 2 and 3 dimensional plots revealed the most structure near this value of delay (see Figure 5). Structure is clearly evident in these plots. Unfortunately, they also reveal a complexity or noise dependence that makes the fine scale structure very difficult to detect. The method of false nearest neighbors[6] (FNN) was chosen as the primary technique for determining the embedding dimension. The results agreed with what was suggested for application with real world data. As shown in Figure 6, the percentage of false neighbors dropped dramatically as the embedding dimension increases from 5 to 6. As will be shown later, this is in at least rough agreement with what was found to be a suitable embedding dimension for determination of Lyapunov exponents or fractal dimensions.

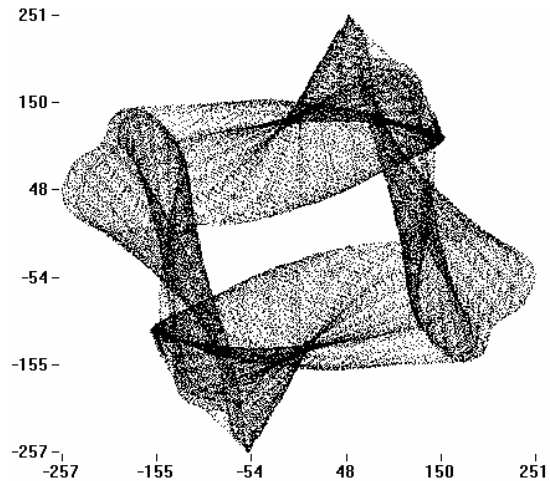


Figure 5. A two dimensional plot of the first 50,000 points from the 50.75Hz flow data with a delay of 11.

4. Fractal Dimension

Analysis was attempted on data sets of varying size and varying embedding dimension. Results of estimations of the correlation dimension for the 59.75Hz data are depicted in Figure 7. A plateau is evident for $\log(\epsilon)$ in the range -1.7 to -3.0 . Here, the correlation dimension can be estimated to be between 1.1 and 1.5. This is a fairly low dimensional system and thus it should be relatively easy to manipulate. Although this value agrees roughly with the choice of embedding dimension, more analysis was necessary to confirm the results.

Figure 8 presents the results of our calculations performed on step motor data. Displayed are estimates of the first four generalized entropies for varying box size with an embedding dimension of 4. Additional tests were also performed for the embedding dimensions 3-6, and for the next four generalized entropies. The results indicated that, for $p > q$, $D(p) \leq D(q)$, which agrees with theory.

For large box size, the box counting dimension varies widely from the others, since the box counting dimension $D(0)$ is more susceptible to errors. It is also a poor quantity to use since it says nothing about the density of the attractor, only about its shape. However, the box counting dimension and all the others converge in the mid-region, before diverging slightly and then dropping to zero (due to data set size). It is this mid region that parallels the plateau region of the Grassberger-Proccacia algorithm[7, 8].

The estimates for fractal dimension ranged from 1.8 to 2.2, for all fractal dimensions calculated when embedding dimension was greater than or equal to 4. With the exception of the box counting dimension, this was true for all of the first four generalized dimensions. The correlation dimension, for instance, was estimated at $D(2) = 2.05 \pm 0.2$, where error was estimated based on the fluctuation of the slope of the entropy in the mid region. This agrees with our choice of 4 for the embedding dimension, and is also in rough agreement with the result from the Grassberger-Proccacia algorithm

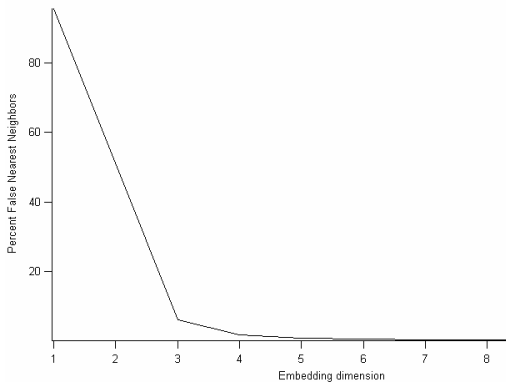


Figure 6. Results of the FNN routine as applied to the 50.75Hz flow data. An appropriate embedding dimension is found when the percentage of false near neighbors drops to a value near zero. This indicates that the embedding dimension should be at least 4.

A fractal dimension of up to 2.5 indicates that an embedding dimension as high as 5 may be necessary, but as is often the case, a lower embedding dimension may be used.

5. Lyapunov Exponents

Before determination of Lyapunov exponents was attempted, the flow data was embedded with a delay of 13, as suggested by the false nearest neighbors routine, the autocorrelation function and the mutual information function. Fractal dimension was estimated as between 2 and 4, so a local embedding dimension of 4,5 or 6 was chosen, yielding 3, 4, or 5 exponents in the calculation of the full spectra. As shall be seen, this is in agreement with the observation that the sum of the exponents must be negative.[9]

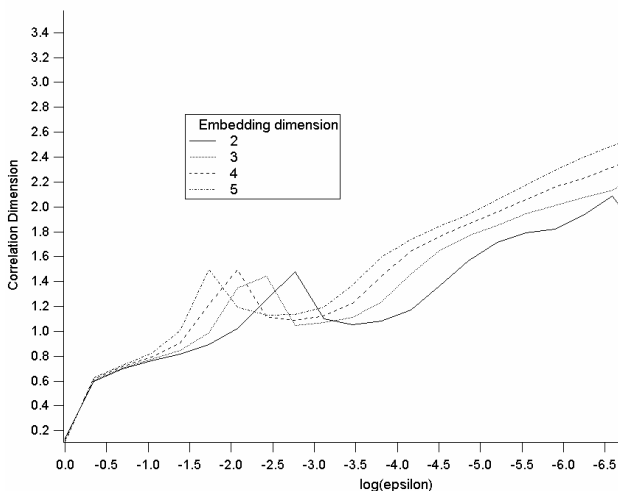


Figure 7. Estimates of the correlation dimension for the 59.75Hz flow data. The correlation dimension is estimated from the slope of $\log(C(\epsilon))$ vs. $\log(\epsilon)$. It can be estimated from the plateau region of the plot, where it is between 1.1 and 1.5.

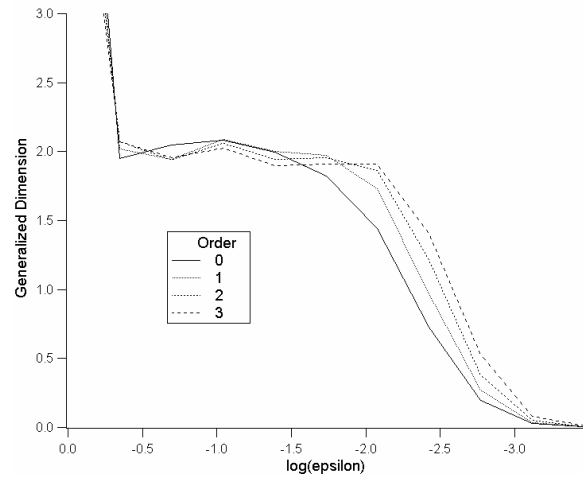


Figure 8. The first 4 generalized entropies. The values are estimated as $D(0) = 2.08 \pm 0.1$, $D(1) = 2.09 \pm 0.1$, $D(2) = 2.05 \pm 0.2$ and $D(3) = 2.02 \pm 0.2$. Each of these was calculated using the 50.75Hz flow data embedded in 4 dimensions.

The Eckmann-Ruelle[10] method was used to determine Lyapunov spectra. The folding of the attractor brings diverging orbits back together. So any effects of nonlinearities will most likely serve to move all exponents closer to zero. Hence a slight underestimate of the positive exponents was expected.

#	embed dim	λ_1	λ_2	λ_3	λ_4
3	3	0.404	0.044	-0.323	
3	4	0.051	-0.033	-0.228	
3	5	-0.005	-0.044	-0.187	
4	4	0.111	0.014	-0.047	-0.306
4	5	0.021	-0.009	-0.045	-0.266

Table 1. Estimation of Lyapunov exponents for the 59.75Hz flow data. The bold faced selection represent the best estimates of the exponents, since it has an exponent closest to zero and the sum of the exponents is negative.

In Table 1 results of exponent calculations are provided. The exponents are given in units of 1/time, where the time scale is defined so that the time between samples is 1. Many more calculations were performed until a reasonable and stable parameter regime was found for both methods. Note that the zero exponent snaps into place for appropriate parameter settings.

Several of our criteria are determined immediately upon inspection. The zero exponent was identified with a high degree of accuracy. The sum of the exponents is negative, while the sum of the first two is positive. This indicates that a fractal dimension between 2 and 3 was a reasonable estimate.

Sectioning the data introduced additional noise and measurement of exponents from the section was even more uncertain. Thus it was not possible to get agreement between exponent estimates from the section and from the flow, nor was it expected. However, Lyapunov spectrum estimates from Poincare section data were estimated as $\lambda_1=0.466$, $\lambda_2=-0.056$ and $\lambda_3=-0.692$.

We note that the estimates here are scaled from the estimates provided in Table 1 because the sampling rate is different.

6. Unstable Periodic Orbits and Control

The identification of unstable periodic orbits (UPOs) plays a critical role in many chaos control algorithms. Most standard chaos control algorithms attempt to control the system onto a UPO while operating within the chaotic regime [11, 12]. Small time-dependent perturbations applied to an accessible parameter may then be used to force the system onto the stable manifold and hence enforce stability and periodic behavior. The drive frequency is the most preferable candidate to use as the varied parameter in a control scheme. This is because it is easily adjustable and, as depicted in Figure 2, a small change in drive frequency yields appropriate changes in the dynamics.

Figure 9 depicts the identification of a period 1 orbit in the Poincare sectioned data. The arrow pointing toward the fixed point (period 1 orbit) indicate a region which is mapped near the fixed point. The arrows pointing away show the direction of the unstable manifold. Control algorithms simply need to adjust the frequency so as to force the dynamics towards the stable manifold that lies orthogonal to these arrows. Furthermore identification of such unstable periodic orbits in occasional proportional feedback control schemes[13], tracking and targeting of trajectories[14], and in the identification of symbolic dynamics[15, 16].

7. Coexisting Attractors and Parameter Drift

When the dynamics change over time in an experimental system it is often difficult to determine the cause. Consider the dynamics observed in the sectioned data file gathered at 58Hz. In Figure 10 we see what appears to be a chaotic attractor. For the first 4000 cycles, the motion of the step motor is along this chaotic trajectory. However, the last 10,000 points gathered clearly indicate that the motion has settled down into period 2 behavior (Figure 11).

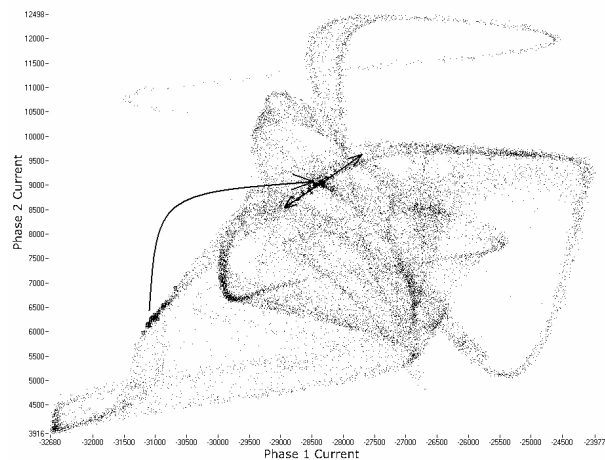


Figure 9. Identification of an unstable periodic orbit (period 1) at 58.6Hz.

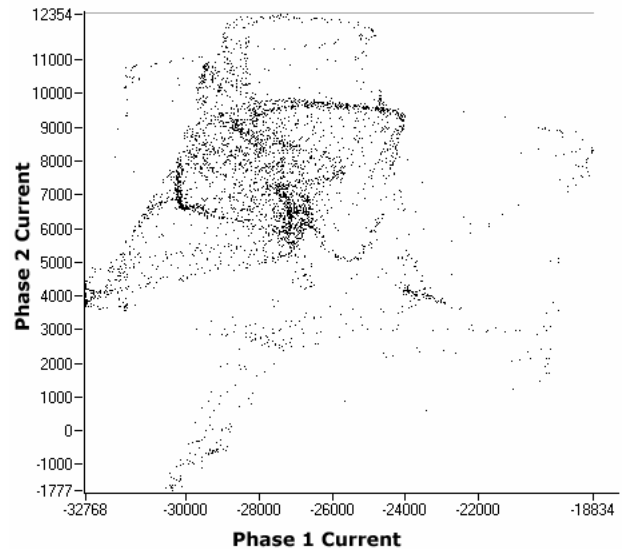


Figure 10. A plot of the first 4,000 data points in the 20,000 point file of sectioned data gathered at 58Hz.

The reason for this change is unclear. First, a stable periodic orbit may exist in conjunction with a chaotic attractor. This orbit resides close to a rarely visited portion of the attractor. Noise in the system is enough for the dynamics to move off the chaotic attractor and onto the periodic orbit.

A second possibility is that a slight change in the parameters has occurred. This change results in a completely different dynamic behavior. Alternatively, an intermittent chaotic behavior might occur, and we have only witnessed one transition in the system. A final more speculative option is that Figure 10 depicts a transient stage. It doesn't represent an attractor at all, but simply the dynamics before settling onto the stable period 2 orbit.

However, parameter drift as the sole cause is an unlikely option. This would indicate that one would expect to see a continued drift in the dynamics, or possibly a return to the initial dynamics. This was not observed. Furthermore analysis of nonstationarity of the windowed mean and windowed standard deviation indicated a relatively sudden change in the dynamics, with little drift before or after that change. Intermittent chaotic behavior is possible, but no return to chaotic behavior was observed. Finally, transient dynamics *were* observed, but only for the first few data points. Figure 10 depicts the dynamics after the system had settled from initial conditions to confined chaotic dynamics.

Thus it is likely that this system exhibits coexisting attractors. This is further confirmed by the fact that a comparison of Figure 10 and Figure 11 reveals that the period 2 orbit is indeed near a rarely visited portion of the attractor. This provides an explanation for why atleast 4,000 iterates were required before the dynamic behavior changed.

Coexisting attractors is highly advantageous for the purposes of control. Should one wish for the motor to exhibit nonchaotic behavior at this frequency, one need only push the system onto the stable periodic orbit. Further control is only required if the noise in the system

is large enough that the dynamics is moved beyond the attracting region of the nonchaotic orbit. Thus a much weaker control may be applied, and applied far less frequently, than in the case of stabilization onto unstable orbits within a chaotic attractor. Conversely, control algorithms may be used to control the system away from the periodic orbit and onto the chaotic attractor. This and similar schemes are often termed *maintenance of chaos*[17].

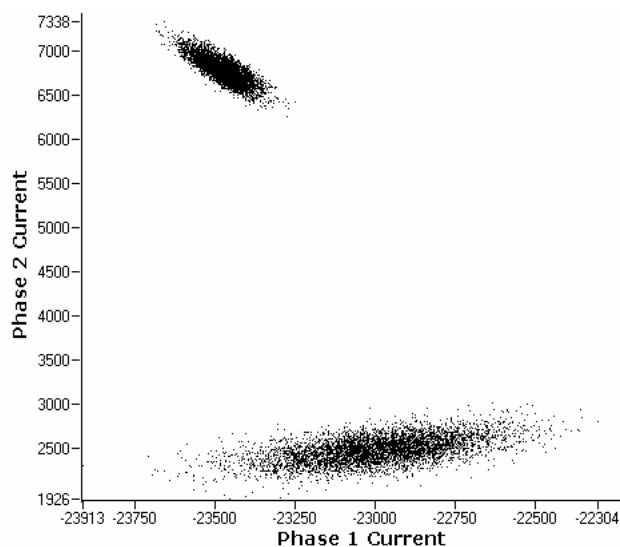


Figure 11. A plot of the last 10,000 data points in the 20,000 point file of sectioned data gathered at 58Hz.

8. Conclusion

The data from the step motor appears to represent a four dimensional (three dimensional when sampled at the drive frequency) system with one positive Lyapunov exponents. This system may therefore be considered low dimensional and chaotic. As such, computation of fractal dimension and of Lyapunov exponents is possible and accurate. Consistency was achieved between results using various methods of analysis. Although the data appeared nonstationary, it is still an excellent system for analysis. This is because the system has only minimal dependence on external factors such as temperature. Furthermore it exhibits a rich range of dynamics, including coexisting attractors, band structures and periodic windows.

Control may be applied to allow the step motor to operate as desired within the chaotic regime. Tracking and maintenance should also be possible, since the appropriate dynamics have been found for the application of several well-known algorithms.

References

1. Pera, M.-C., B. Robert, and D. Guegan. *Electric step motor: nonlinear dynamics and estimation of embedding dimension*. in *5th Experimental Chaos Conference*. 1999. Boca Raton, Florida: World Scientific.
2. Pera, M.C., B. Robert, and C. Goedel. *Quasiperiodicity and Chaos in a Step Motor*. in *8th European Conference on Power Electronics and Applications*. 1999. Lausanne, Switzerland.
3. Fraser, A.M., *Reconstructing Attractors from Scalar Time Series: A Comparison of Singular System and Redundancy Criteria*. *Physica D*, 1989. **34**: p. 391-404.
4. Fraser, A.M. and H.L. Swinney, *Independent coordinates for strange attractors from mutual information*. *Phys. Rev. A*, 1986. **33**(2): p. 1134-1140.
5. Reiss, J.D., N. Mitianoudis, and M.B. Sandler. *Computation of Generalized Mutual Information from Multichannel Audio Data*. in *110th Convention of the Audio Engineering Society*. 2001. Amsterdam, The Netherlands.
6. Kennel, M.B., R. Brown, and H.D.I. Abarbanel, *Determining embedding dimension for phase-space reconstruction using a geometrical construction*. *Phys. Rev. A*, 1992. **45**: p. 3403-3411.
7. Grassberger, P. and I. Procaccia, *Measuring the strangeness of strange attractors*. *Physica D*, 1983. **9**: p. 189-208.
8. Grassberger, P. and I. Procaccia, *On the characterization of strange attractors*. *Phys. Rev. Lett.*, 1983. **50**: p. 346-349.
9. Crutchfield, J.P. and N.H. Packard, *Symbolic dynamics of noisy chaos*. *Physica D*, 1983. **7**: p. 201.
10. Eckmann, J.-P., et al., *Liapunov Exponents from Time Series*. *Phys. Rev. A*, 1986. **34**: p. 4971-4979.
11. Ott, E., *Controlling chaos: Review and some recent developments*, in *LEOS '95. IEEE Lasers and Electro-Optics Soc., 8th Annual Meeting 1995. Conf. Proc. (Cat. No. 95CH35739)*. 1995, IEEE 1995: New York. p. 31-32.
12. Ott, E., C. Grebogi, and J.A. Yorke, *Controlling Chaos*. *Phys. Rev. Lett.*, 1990. **64**: p. 1196-1199.
13. Senesac, L.R., et al., *Controlling chaotic systems with occasional proportional feedback*. *Rev. Sci. Instr.*, 1999. **70**(3): p. 1719-1724.
14. Shinbrot, T., et al., *Using the sensitive dependence of chaos (the "butterfly effect") to direct trajectories in an experimental chaotic system*. *Phys. Rev. Lett.*, 1992. **68**: p. 2863-2866.
15. Lathrop, D.P. and E.J. Kostelich, *Characterization of an experimental strange attractor by periodic orbits*. *Phys. Rev. A*, 1989. **40**: p. 4028-4031.
16. Mischaikow, K., et al., *Construction of symbolic dynamics from experimental time series*. *Phys. Rev. Lett.*, 1999. **82**(6): p. 1144-1147.
17. In, V., et al., *Experimental maintenance of chaos*. *Phys. Rev. Lett.*, 1995. **74**(22): p. 4420-4423.